Characterization of High-Velocity Single Particle Impacts on Plasma-Sprayed Ceramic Coatings

Jarkko Kiilakoski [1,*]

Email jarkko.kiilakoski@tut.fi

Matti Lindroos [1]

Marian Apostol [1]

Heli Koivuluoto [1]

Veli-Tapani Kuokkala [1]

Petri Vuoristo [1]

[1] Department of Materials Science, Tampere University of Technology, P.O. Box 589, 33101 Tampere, Finland

This is a post-peer-review, pre-copyedit version of an article published in Journal of Thermal Spray Technology. The final authenticated version is available online at:

http://dx.doi.org/10.1007/s11666-016-0428-2

Abstract

High-velocity impact wear can have a significant effect on the lifetime of thermally sprayed coatings in multiple applications, e.g., in the process and paper industries. Plasma-sprayed oxide coatings, such as Cr_2O_3- and TiO_2-based coatings, are often used in these industries in wear and corrosion applications. An experimental impact study was performed on thermally sprayed ceramic coatings using the High-Velocity Particle Impactor (HVPI) at oblique angles to investigate the damage, failure, and deformation of the coated structures. The impact site was characterized by profilometry, optical microscopy, and scanning electron microscopy (SEM). Furthermore, the connection between the microstructural details and impact behavior was studied in order to reveal the damage and failure characteristics at a more comprehensive level. Differences in the fracture behavior were found between the thermally sprayed Cr_2O_3 and TiO_2 coatings, and a concept of critical impact energy is presented here. The superior cohesion of the TiO_2 coating inhibited interlamellar cracking while the Cr_2O_3 coating suffered greater damage at high impact energies. The HVPI experiment has proven to be able to produce valuable information about the deformation behavior of coatings under high strain rates and could be utilized further in the development of wear-resistant coatings.

AQ1

Keywords

electron microscopy
fracture
impact wear
thermal spray coatings

wear testing

Introduction

Thermal spraying means depositing a thick coating (from tens of micrometers up to some millimeters) by propelling molten or semi-molten material onto a substrate, where it flattens and solidifies, forming a coating. The coating is formed of splats that have cooled rapidly, in excess of 10^6 K/s for ceramics (Ref 1). The cooling leads to a varying microstructure with several phases, pores, and inclusions of unmolten particles (Ref 1, 2). Thermally sprayed ceramic coatings such as Al_2O_3, Cr_2O_3, ZrO_2-$8Y_2O_3$, and TiO_2 are widely used in applications requiring a surface resistant to corrosion and wear (Ref 3-5). Such applications can be found for example in process and paper industries, where ceramic coatings are used against adhesive wear of fibers (Ref 2, 5). The coatings are most commonly deposited by Atmospheric Plasma Spraying (APS) or High-Velocity Oxy-Fuel (HVOF) spraying. Other beneficial qualities of thermally sprayed ceramic coatings can be high hardness, low friction, resistance to low-angle erosion, electrical insulation, and semiconductivity.

Thermally sprayed ceramic coatings often exhibit microcracking in the direction perpendicular to the substrate, stemming from their brittleness and, as a result, inability to accommodate residual stresses during cooling. This leads to their limited use in applications, which require impact resistance and where ductility is often considered beneficial (Ref 5). Plasma-sprayed Cr_2O_3 coatings are, however, widely used against adhesive and abrasive wear, as well as against corrosion when sealed, whereas TiO_2 coatings are used or researched for their solid-lubrication, electrical conductivity, and photocatalytic properties (Ref 6-8). APS Cr_2O_3 coatings usually have a hardness between 1000 and 1300 $HV_{0.3}$ (Ref 6, 9), while TiO_2 coatings typically have a hardness of around 800 $HV_{0.3}$ sprayed both with APS and HVOF (Ref 10).

The brittleness of ceramic coatings is evidenced by their low ability to resist crack growth, which is indicative of the amount of energy needed to break the material (Ref 11, 12). Due to the large amount of defects in plasma-sprayed coatings, their mechanical properties are often poorer than those of the corresponding bulk materials. For example, the elastic moduli of oxide coatings are estimated to be only 20-40% of those of their bulk counterparts (Ref 5). These properties are in the first place not only related to the feedstock material and the final microstructure of the coatings, but they can also be influenced for example by optimizing the feedstock manufacturing and spray processes. New spray methods and coatings with nanoscale features provide promising new routes for achieving toughness in ceramic coatings (Ref 13).

The wear of thermally sprayed ceramic coatings is largely dependent on the composition of the coating, interlamellar strength, and the porosity and density of microcracks in the microstructure (Ref 14, 15). Additionally, residual stresses may play a certain role in applications where outside stress is imposed on the coating (Ref 16, 17). The stresses can add up or reduce depending on their sign which can accelerate failure. The stresses for plasma-sprayed ceramic coatings have usually been thought of as being tensile (Ref 17-19), although polishing of the coating can induce slight compressive stresses (Ref 17).

Research on the erosion resistance of plasma-sprayed Al_2O_3 and TiO_2 coatings has shown that they

have sufficient resistance against scratching by low-angle erosion due to their high hardness and stiffness, but with right angle impacts the wear rates were increased even fivefold (Ref 20). Indeed, Matikainen et al. (Ref 21) found that, for Al_2O_3 and Al_2O_3-TiO_2 coatings sprayed with HVOF and APS spray processes, the erosion wear rate with a 30° angle was between 25 and 50% of the wear rate with an angle of 90°. The mechanism of material removal by small particles was mainly brittle fracture, preceded by plastic deformation, while for larger particles with the impact angle of 90°, brittle fracture occurred at the interface between the lamellae. Westergård et al. (Ref 22) noted from eroded surfaces of plasma-sprayed Al_2O_3, Al_2O_3-13TiO_2, and Cr_2O_3 that during erosion cracking in the coating follows the path of weak sites in the coating. They suggest that erosion wear is a good measure of the cohesion of the coating (Ref 23).

AQ2

Supporting the above, Takeuchi et al. (Ref 24) found that the erosion resistance of plasma-sprayed TiO_2 is superior to that of Cr_2O_3 at the impact angle of 60°. They also performed a drop test of a steel ball on the coatings at a 45° angle and observed the TiO_2 coating to endure twice as many impacts as the Cr_2O_3 coating. Sparks et al. (Ref 25) have studied the effect of erodents of different shapes and velocities on a silica glass ceramic bulk material in a dry erosion test. They used angular and blocky silica sands of particle sizes 125-150 µm with a gas blast erosion rig. They found that in the tests at low velocities (44 m/s) with rounded particles, a transition in the erosion wear rate took place between the impact angles of 45° and 60°. In higher angles and velocities, the wear of the ceramic was characterized by lateral cracking and flake formation, whereas below the transition point plastic deformation preceded the fracture. To the best of our knowledge, similar studies have not been performed on wear-resistant ceramic coatings, which would reveal the connection between deformation, critical loading conditions, and failure mechanisms. However, it must be recognized that these coatings may not provide the best wear resistance when erosion is the prevailing loading mode. In such applications, cermets such as tungsten and chromium carbides are often preferred due to the possibility of adjusting the amount of hard phase favorable against erosion. (Ref 20).

High-velocity single impact studies have been performed at Tampere Wear Center (TWC) on various materials with the High-Velocity Particle Impactor (HVPI). The test setup has been successfully used for studying impacts in a controlled way for materials such as steels (Ref 26, 27), hybrids (Ref 28, 29), thermally sprayed MMC coatings (Ref 30), and rubbers (Ref 31). Waudby et al. (Ref 30) characterized the high-velocity impacts with various impact velocities on thermally sprayed cermet coatings and concluded that the erosion mechanism is mostly cracking, indicating brittle behavior of the coatings. They also determined the critical level of impact energy above which coating delamination and significant plastic deformation of the substrate were evident. Below this impact energy, the coating cracked and deformed but still stayed somewhat intact and on the substrate, providing protection against further impacts.

In the present study, high-velocity single impact experiments were performed to elucidate the wear characteristics and deformation behavior of two wear-resistant ceramic coatings, i.e., atmospheric plasma-sprayed Cr_2O_3 and TiO_2, in low-angle impacts. These coatings were chosen for their different microstructural characteristics, which are presumed to result in different types of wear behavior. Electron microscopy and profilometry were used to analyze the failure mechanisms and microstructures of the coatings before and after the impact tests.

Materials and Methods

Materials

Conventional chromia (dichromium trioxide, Cr_2O_3) (H.C. Starck, Amperit 704.001) and titania (titanium dioxide, TiO_2) (H.C. Starck, Amperit 782.1) were chosen as coating materials. Both powders were fused and crushed with a nominal powder size of −45 + 22 μm. The powder morphologies are presented in Fig. 1. The coatings were sprayed on low carbon steel (AISI 5120) plates, which were grit-blasted with alumina (grit 36) before spraying. The coatings were produced by using the atmospheric plasma spray (APS) process consisting of a Oerlikon Metco F4-MB-XL torch with a plasma gun and a Plasma Technik A-3000S 4/2 plasma spray system. The spray parameters are presented in Table 1. The TiO_2 coating was sprayed with less power due to its lower melting point (~1857°C vs. ~2330°C for Cr_2O_3) (Ref 11). Both coatings were ground with grit 600 and 1200 SiC papers to thicknesses of 120 μm for TiO_2 and 320 μm for Cr_2O_3 and polished with 3 μm and 1 μm diamond suspensions. In the case of microscopic examination of crack paths, the two thicknesses are not believed to have a significant effect.

Fig. 1

Powder morphologies of the (a) Cr_2O_3 and (b) TiO_2 powders. SEM images

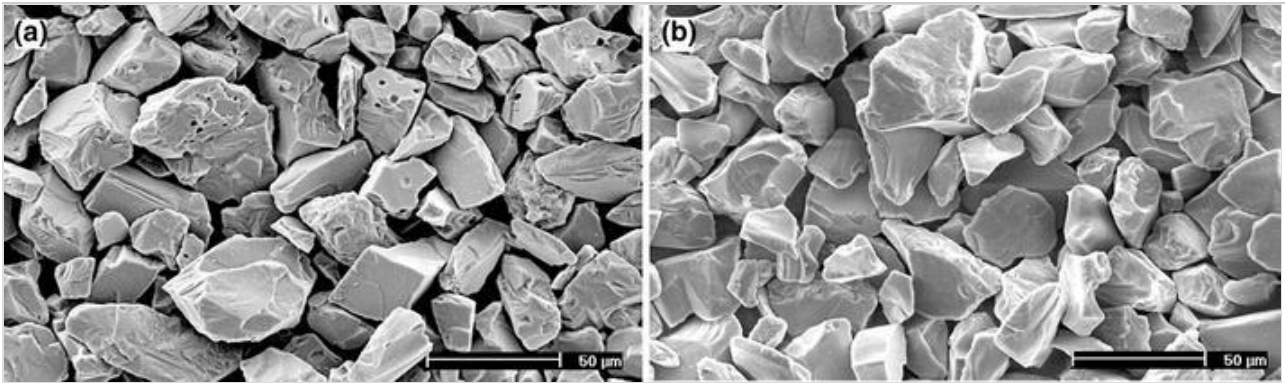

Table 1

Spray parameters used for the APS ceramic coatings

	Cr_2O_3	TiO_2
Current (A)	630	600
Power (kW)	46.2	43.2
Ar/H_2 (slpm)	38/13	47/12
Powder feed (g/min)	53	50
Spray distance (mm)	110	
Surface speed (m/min)	87	

High-Velocity Single Impact Experiment

The experimental setup of the High-Velocity Particle Impactor is illustrated in Fig. 2(a). In the method, compressed air is used to accelerate the projectile in a smooth bore barrel to a predefined

impact velocity, which is measured with a chronograph placed in front of the sample. The material of the spherical projectiles of two different sizes used in the present study is chromium steel. The impact events are recorded with a high-speed camera (NAC, Memrecam fx K5) typically with a 50 µs interframe rate to calculate the exit velocities of the projectiles after the impact. An example of overlaid and processed high-speed camera images is presented in Fig. 2(b) and the used test parameters in Table 2.

Fig. 2

(a) A schematic drawing of the HVPI setup (Ref. 32) and (b) four overlaid high-speed images presenting a 30° impact incident; outlines of the projectiles are shown for clarity

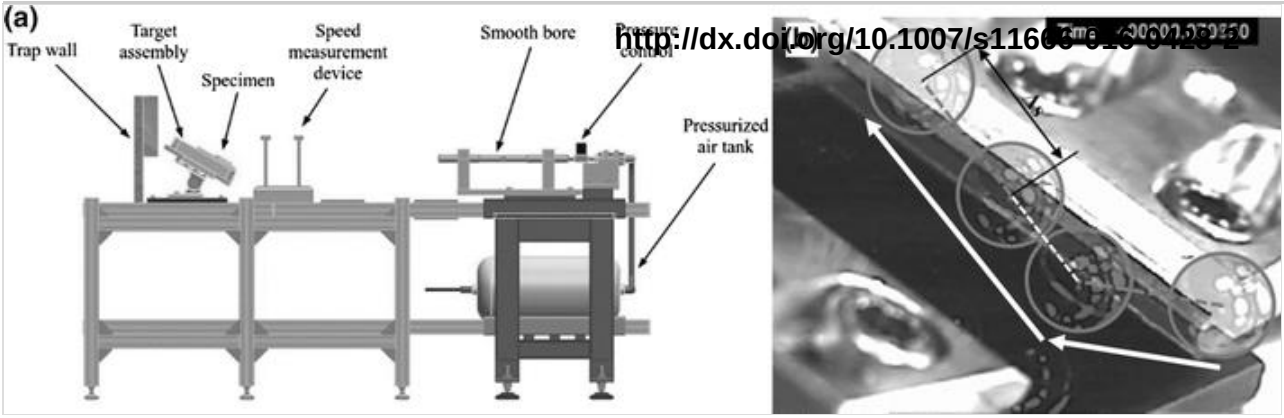

Table 2

Test parameters and the measured impact velocities in the HVPI single impact experiments

	Impact angle, °	Diameter of the projectile, mm	Mass of the projectile, g	Incident velocity of the projectile, m/s
Cr_2O_3 coating	15	9	2.9	34.7 ± 0.5
		5	0.51	48.0 ± 0.0
	30	9	2.9	34.3 ± 0.5
		5	0.51	47.3 ± 0.5
TiO_2 coating	15	9	2.9	35.0 ± 0.0
		5	0.51	47.7 ± 0.5
	30	9	2.9	35.0 ± 0.0
		5	0.51	47.3 ± 0.5

The incident velocities, v_{inci}, were measured with a ballistic chronograph placed in front of the target assembly, and the initial kinetic energies, E_{inci}, were calculated. The exit velocity v_{exit}, the distance traveled by the projectile in a certain time increment ($\Delta s/\Delta t$), and thus reflected kinetic energy E_{refl} were determined by image analysis from the high-speed images (Fig. 2b). The fraction of energy dissipated E_d during the incident was calculated as

$$E_d = E_{inci} - E_{refl} = \frac{1}{2} m_p (v_{inci} - v_{exit})^2 \quad (1)$$

where m_p is the mass of the projectile.

Characterization Methods

The microstructures of the powders and coatings as well as the impact craters were investigated by Scanning Electron Microscope (SEM) Philips XL30 equipped with Energy Dispersive x-ray (EDX) microanalyzer. Microhardnesses of the coatings were measured as averages of ten indentations with a microhardness tester Matsuzawa MMT-X7 using loads from 100 gf ($HV_{0.1}$) to 1000 gf (HV_1). In addition, Vickers indentations were also done with loads ranging from 2000 gf (HV_2) up to 30,000 gf (HV_{30}). The indents were studied with SEM. The amount of cracks in the coating resulting from the impact was determined with optical image analysis (ImageJ) from SEM (BSE)-images from the surface of the impact sites. The surface topologies of the impact craters were analyzed using a Wyko NT-1100 optical profilometer. A special Matlab code was developed to analyze the profilometer data, while Minitab 15 (Minitab Inc.) was used for the statistical analysis of the energy dissipation behavior.

Results and Discussion

Microstructures

Figure 3 presents the original microstructures of the plasma-sprayed Cr_2O_3 (a,b) and TiO_2 (c,d) coatings. Both coatings exhibit both lateral and horizontal cracks stemming from the tensile residual stresses, which are typical for plasma-sprayed ceramic coatings (Ref 5, 33). In the TiO_2-coating, some horizontal microcracks are present, but in general the lamellae seem to be bonded better with no pronounced interfaces. A small amount of voids and pullouts is present in both coatings.

Fig. 3

Microstructures of the plasma-sprayed Cr_2O_3 (a and b) and TiO_2 (c and d) coatings. SEM BSE images

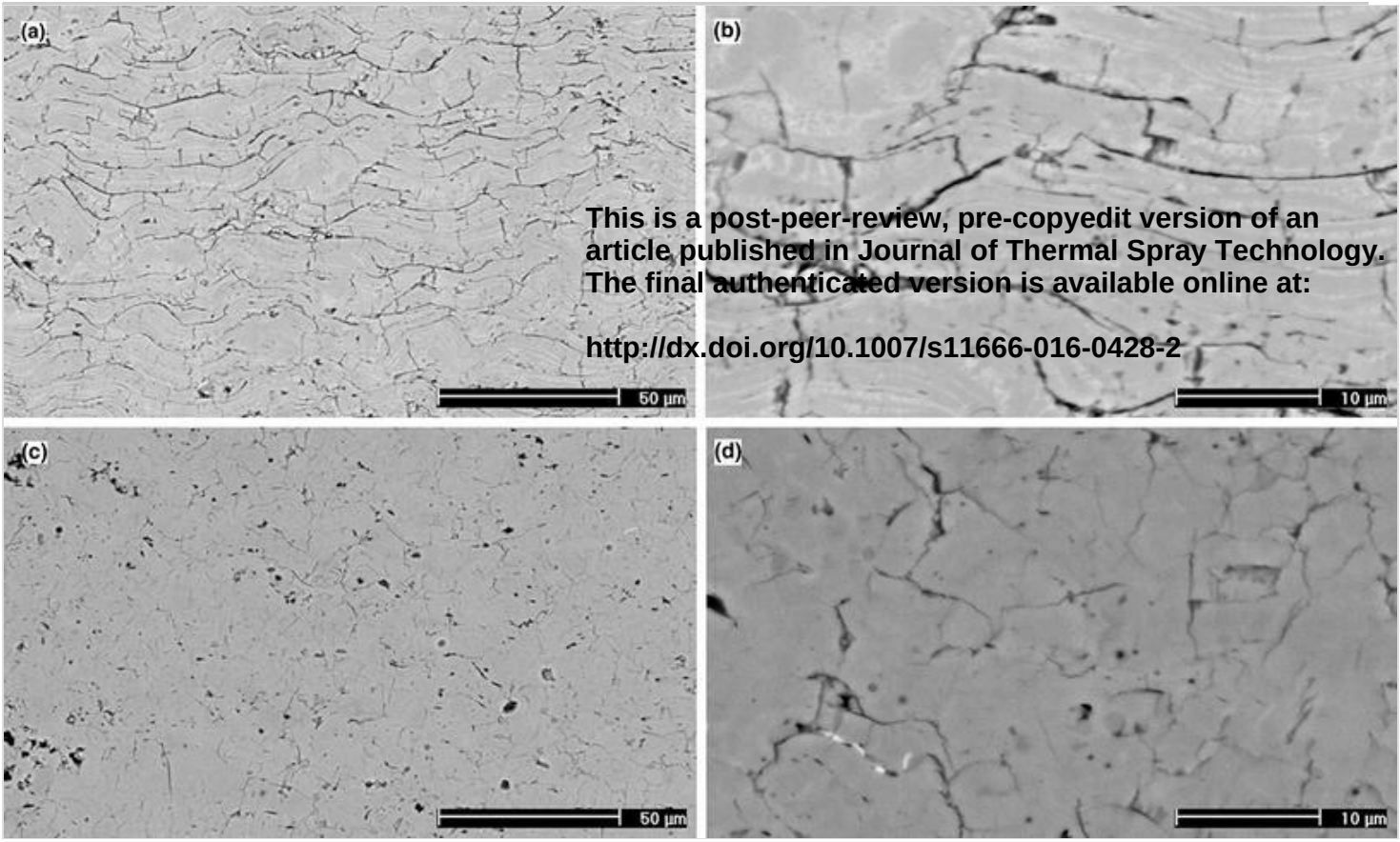

The extensive interlamellar cracking observed in the Cr_2O_3 coating is often attributed to its high melting point and high tendency to form gaseous phases during spraying. (Ref 34) This vapor readily condensates on the sample surface, weakening the bond between the already sprayed and subsequent lamellae, thus leading to poor cohesion. The intra-splat cracks are due to the rapid quenching of the splats and the inability of the ceramic splats to deform. Since TiO_2 is a less refractory ceramic, the coatings formed from it are often less porous, as is the case here as well.

High-Velocity Single Impact Experiments

The results of the HVPI tests are presented in Table 3, where the impact angle, ball diameter, and exit velocity are presented along with the incident and dissipated energies. Additionally, the amount of cracking was determined with optical image analysis from the SEM images of the impact craters. As seen in Table 3, the energy dissipation depends heavily on the test conditions for both materials. In all cases except for the one with the greatest initial energy (9 mm ball, 30° impact angle), the TiO_2 coating dissipated more energy than the Cr_2O_3 coating. This correlates very well with the amount of cracks found on the surface of the samples. The percentage of energy dissipation is, interestingly enough, quite similar at the 15° angle for both projectile sizes. However, at 30°, the smaller projectile loses approximately 50% more of its initial energy than the larger projectile.

Table 3

Results of the HVPI tests

	Angle, °	D_{ball}, mm	V_{exit}, m/s	E_{inci}, J	E_d, J	E_d, %	Amount of cracks, %
Cr_2O_3	15	9	30.2 ± 0.7	1.74 ± 0.06	0.42 ± 0.03	24.2 ± 1.9	0.5
		5	41.2 ± 1.3	0.59 ± 0.00	0.15 ± 0.03	26.2 ± 4.5	0.125
	30	9	27.4 ± 0.3	1.74 ± 0.06	0.69 ± 0.16	39.6 ± 9.6	1.6
		5	35.7 ± 0.5	0.57 ± 0.01	0.25 ± 0.03	43.6 ± 3.6	0.2
TiO_2	15	9	29.9 ± 0.1	1.78 ± 0.00	0.48 ± 0.01	27.2 ± 0.7	0.6
		5	40.6 ± 1.1	0.58 ± 0.01	0.16 ± 0.01	27.5 ± 2.7	0.4
	30	9	28.9 ± 0.2	1.78 ± 0.00	0.56 ± 0.02	31.6 ± 1.1	0.9
		5	33.7 ± 0.6	0.57 ± 0.01	0.28 ± 0.02	49.2 ± 2.4	0.9

'Angle' is the impact angle of the projectile, d_{ball} is the diameter of the projectile, v_{exit} is the velocity of the projectile after the impact, and E_d is the dissipated energy. E_d (%) is the ratio of dissipated energy to incident energy

Figure 4(a) presents the dissipated energy for both impact angles and projectile sizes. In the boxplot, the outline of the boxes represents the range of results and the line in the middle the median. From these results, it is clear that there is a change in the relative amount of energy dissipation with the strongest impact for the Cr_2O_3-coating, as described above. Figure 4(b) shows the relationship between the measured energy dissipation and the identified percentage of deformation-induced cracks in the microstructure. The increase in the amount of cracks indicates that a reasonable part of the energy is consumed in the fracturing process. Since increase in the amount of impact energy that the coating absorbs increases the amount of cracking, it seems plausible that the main mechanism of energy dissipation is indeed cracking.

Fig. 4

(a) Dissipated energies at 15° and 30° impact angles with two projectile sizes for both coatings. (b) Relationship between dissipated energy and amount of deformation-induced cracks in the microstructure

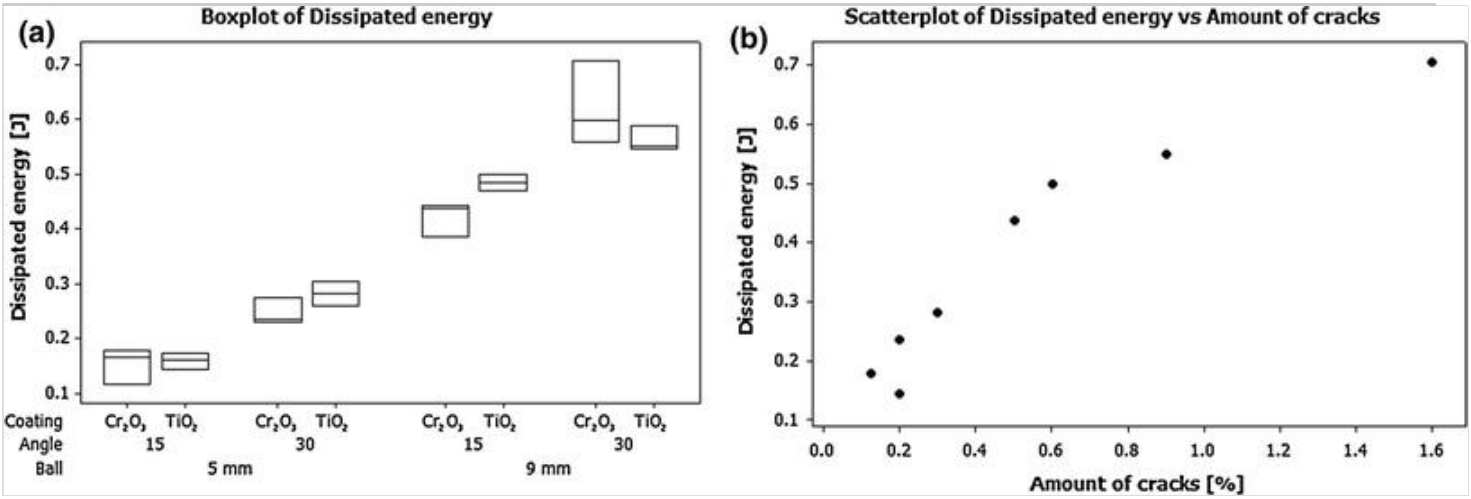

When examining more closely the SEM images in Fig. 5, extensive cracking in the bottom of the crater of the impact can be observed. Similar behavior has been reported for example by Waudby et al. (Ref 30). Adhesion of varying extent between the coating and the projectile was a common denominator for all impacts, as implied by the small amount of iron on the bottom of all craters. The Cr_2O_3 coating showed less absorbed energy during the impacts when smaller projectile size and lower impact angles were used. This indicates that the Cr_2O_3 coating is capable of reflecting the impact energy without severe cracking, i.e., higher hardness/strength allows better storage of elastic energy instead of cracking or failure. However, quite the opposite happens when the coating is no longer able to withstand the deformation and cracking prevails: the fracture process consumes more energy, which can be seen as pronounced energy dissipation. Hassani-Gangaraj et al. (Ref 26) found that for steels the percentage of dissipated energy at the 30° impact angle is double compared to 15°, suggesting a strong correspondence to the test conditions as also witnessed here to a lesser extent. In the present case, the incident energy with 9-mm projectiles is high enough to cause cracking, which is especially evident at the higher impact angle. This also indicates that the observed behavior relates to a certain critical limit before more severe failure occurs, similarly as observed by Sparks et al. in (Ref 25). On the other hand, TiO_2 generally shows slightly higher energy dissipation into the coating/substrate-system as well as cracking but not a distinctive transition to severe cracking, probably due to its better structural cohesion, as seen in the cross section in Fig. 3.

Fig. 5

Surface of the impact craters: (a) TiO_2, 5 mm, 15°; (b) Cr_2O_3, 5 mm, 15°; (c) TiO_2, 9 mm, 30°; and (d) Cr_2O_3, 9 mm, 30°. SEM BSE images

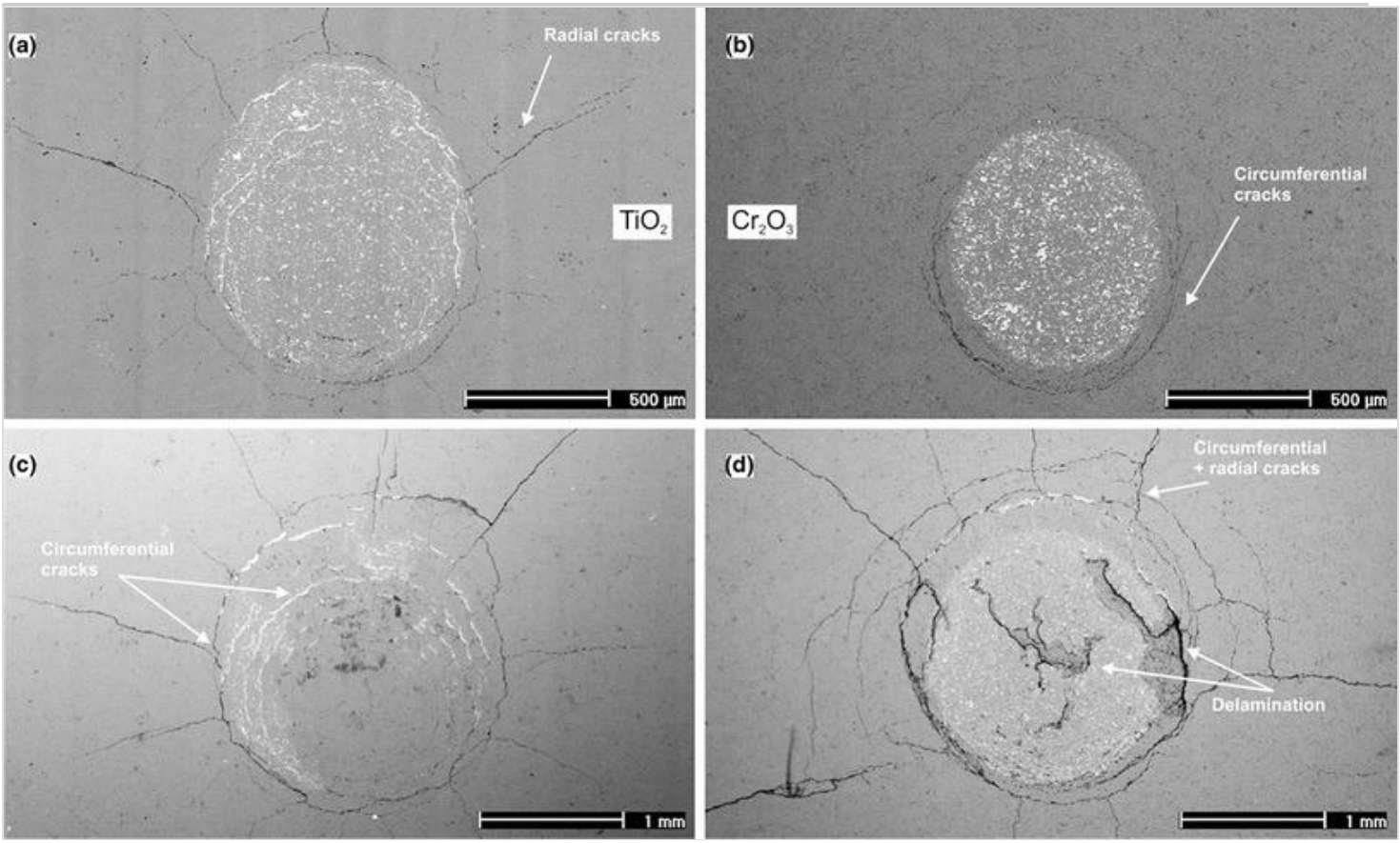

2D-profiles of the impact craters as shown in Fig. 5 are presented in Fig. 6. The difference in the

depth of the craters between the two coatings is noticeable. With the 5-mm projectile, the maximum depths of the craters in the Cr_2O_3 and TiO_2 coatings are 10 and 35 µm, respectively. This is in good agreement with what can be seen in Fig. 5(a) and (b), where the damage in Cr_2O_3 is very limited in comparison to TiO_2. However, with the larger projectile, the maximum depths are from 100 µm (Cr_2O_3) to 85 µm (TiO_2). This can partly be attributed to the extensive delamination in the middle of the crater in the Cr_2O_3 coating. Nevertheless, the result could be expected based on the amount of cracking visible in Fig. 5(d). Also the shape of the crater in the Cr_2O_3 with the larger projectile is similar to that of the craters in both TiO_2 impact sites, while the smaller projectile creates a crater with a shape of a dent without a clear crater lip.

Fig. 6

2D-profiles of four impact craters: (a) TiO_2, 5 mm, 15°; (b) Cr_2O_3, 5 mm, 15°; (c) TiO_2, 9 mm, 30°; and (d) Cr_2O_3, 9 mm, 30°. The arrow shows the impact direction

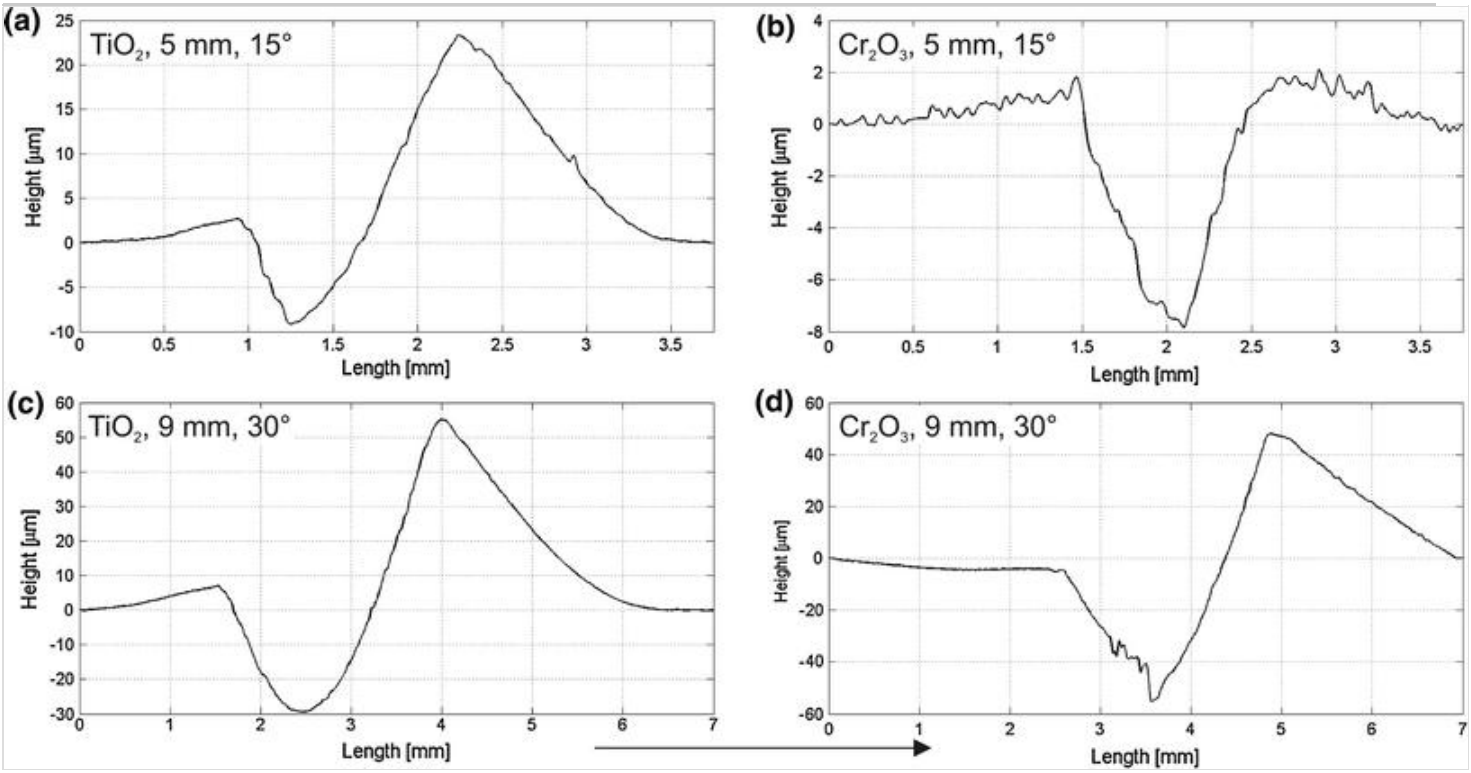

The cross sections of the impact craters with the lighter impacts (5-mm projectile and 15° angle) are presented in Fig. 7. It is clear from Fig. 7(a) that the Cr_2O_3-coating stayed largely intact, although a slight dent and cohesive cracking occurred directly under the impact site. The TiO_2-coating (Fig. 7b), on the contrary, suffered severe damage in the form of vertical (circumferential) cracking and delamination at the substrate-coating interface.

Fig. 7

SEM images of the cross sections of the impact craters created by the 5-mm projectile at a 15° angle in (a) Cr_2O_3-coating and (b) TiO_2-coating. ~~The arrow shows the impact direction~~Impact direction in both images is left-to-right as also shown by the arrow

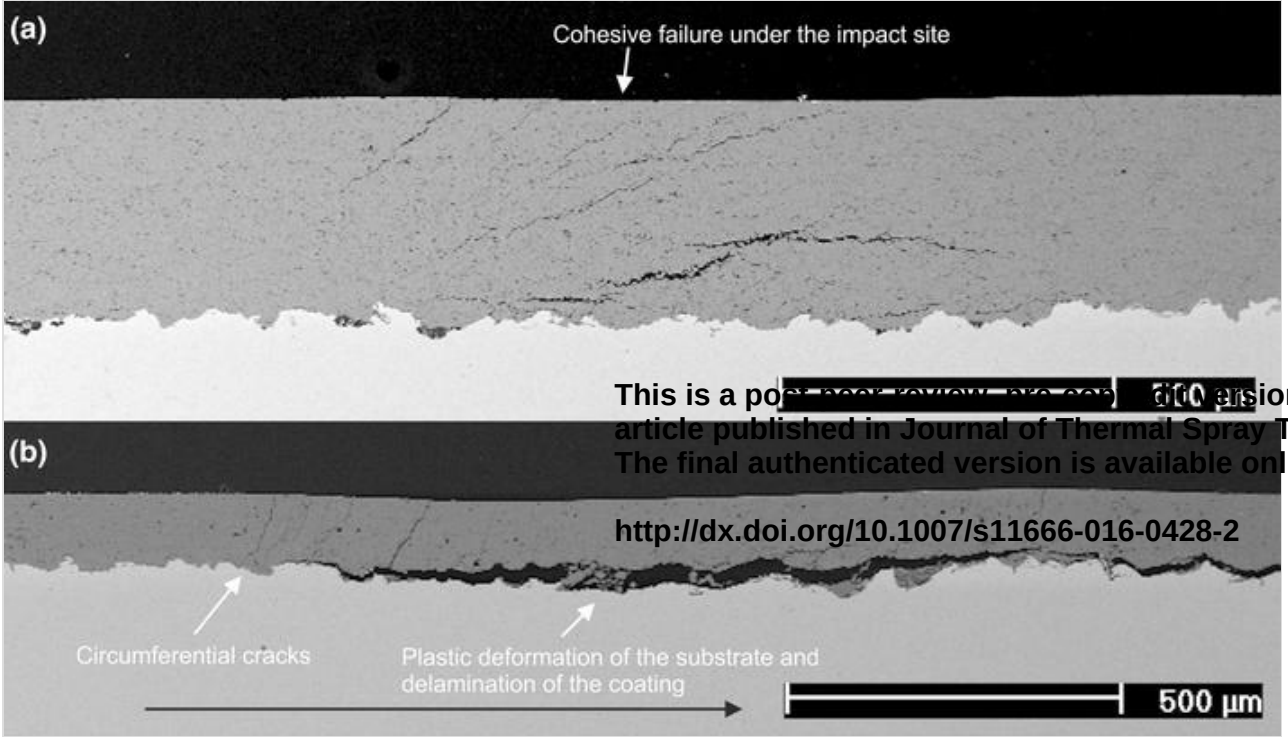

Figure 8 presents the cross sections of the impact craters created by the highest impact energies (9-mm projectile and 30° angle). Both coatings exhibit delamination from the substrate and circumferential cracking that is also seen in Fig. 5(c) and (d). Heavy interlamellar cracking can also be seen on the exit side of the impact crater, probably created by the plastic deformation of the substrate clearly visible in Fig. 8. Differing from the TiO_2 coating (Fig. 8c and d), in the Cr_2O_3 coating (Fig. 8a and b), heavy decohesion occurs within the coating in the center of the crater. The largest of these cracks seems to be almost perpendicular to the impact direction of 30°. The TiO_2 coating does not exhibit such behavior; instead, the coating has detached from the substrate but internally it remains essentially intact. No significant difference between the two different impact incidents can be observed for the TiO_2-coating, and the failure mode seems to be essentially the same, as evidenced by Figs. 7(b) and 8(b). The effect of residual stresses on the cracking is yet to be determined; however, it is believed to be negligible considering the high-energy impact in comparison with intralamellar cohesion of the coatings.

Fig. 8

SEM-images of the cross sections of the impact craters created by the 9-mm projectile at a 30° angle in (a, c) Cr_2O_3-coating and (b, d) TiO_2-coating. Impact direction in all images is left-to-right as also shown by the arrow

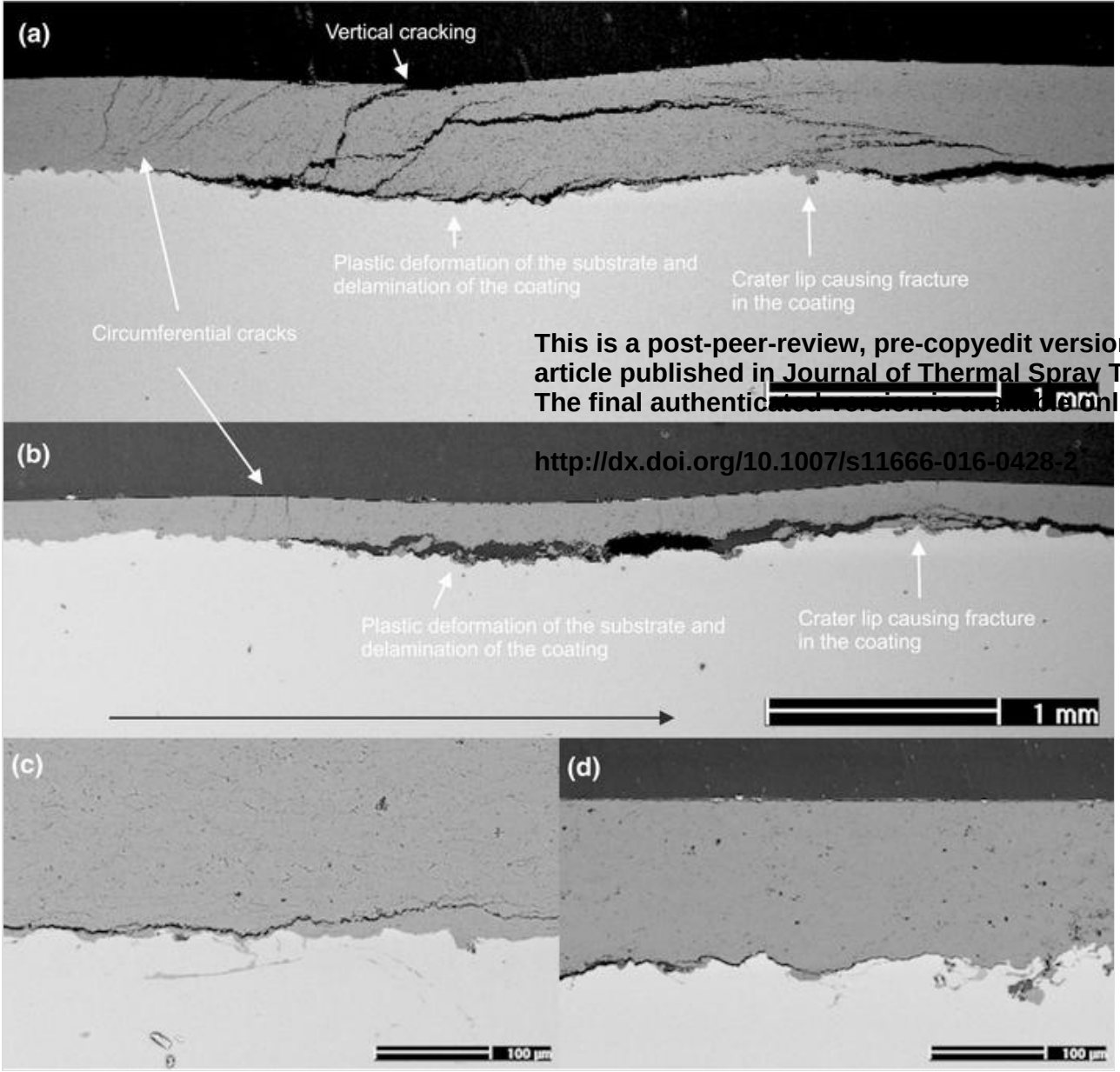

When comparing the behavior of the interfacial cracks in Fig. 8(c) and (d), it seems that in the Cr_2O_3 coating sufficiently far from the crater the cracks transform from an interfacial crack into an interlamellar crack. This phenomenon may be explained with the well-known equation (Ref 11, 35) for fracture toughness, i.e.,

$$\sigma_f \sqrt{\pi c_{crit}} \geq \sqrt{2\gamma Y} = K_{IC} \qquad 2$$

where σ_f is the stress at fracture, c_{crit} is the critical crack length, γ is the intrinsic surface energy of the material, and Y is Young's modulus. In Eq 2, the stress intensity factor on the left hand side has to overcome the critical stress intensity factor, K_{IC}, which is a function of Young's modulus and the surface energy required when creating two new surfaces as the crack propagates. In fact, for purely brittle solids, 2γ is the limit that the toughness of the material (G_c) approaches (Ref 11). Disregarding possible local differences in the elastic modulus within the Cr_2O_3-coating, it seems that the energy required to create the new surfaces (γ) is lower between the lamellae than at the interface. This phenomenon only appears as the energy of the crack diminishes, possibly due to the elastic waves that propagate on the substrate surface postimpact and make the interface a more favorable crack path. In the practical applications of thermal-sprayed ceramic coatings, metallic interlayers (bond coats) are

often used between the ceramic coating and the substrate to improve the adhesion between the coating and the substrate (Ref 2). The situation would be more complex and likely the crack path would look somewhat different if a bond coat was applied, but we can definitely compare the two impact incidents in both materials. While the aforementioned inspection of the crack path is valid for the Cr_2O_3 coating, this behavior cannot be seen in the TiO_2 coating. Instead, the crack in the latter case simply terminates at the interface. This leads to a conclusion that the cohesion of the TiO_2 coating is apparently higher, i.e., the energy required to break an interlamellar bond is higher than the one required to break the adhesion between the coating and the substrate.

Vickers Indentations

Both coatings were indented on the surface with a Vickers indenter using loads from 100 grams to 30 kg. The hardness values were determined from the indents made with loads under 1000 grams and are plotted in Fig. 9. The hardness of Cr_2O_3 is higher than that of TiO_2 at all loads, especially at the smaller ones: $HV_{0.1}$ = 1311 ± 101 for Cr_2O_3 and 905 ± 72 for TiO_2 leads to a difference of 406 $HV_{0.1}$ in hardness. With the 1000-gram load, for example, the difference is only 286 HV_1 (1115 ± 92 vs. 830 ± 35). Hence, the measured hardness of the Cr_2O_3-coating is higher but the difference decreases when using heavier loads in the measurement, which indicates that cohesion of the coating, not the material property, is the determining factor of coating hardness with high loads.

Fig. 9

Vickers hardness values measured for the Cr_2O_3 and TiO_2-coatings with different loads

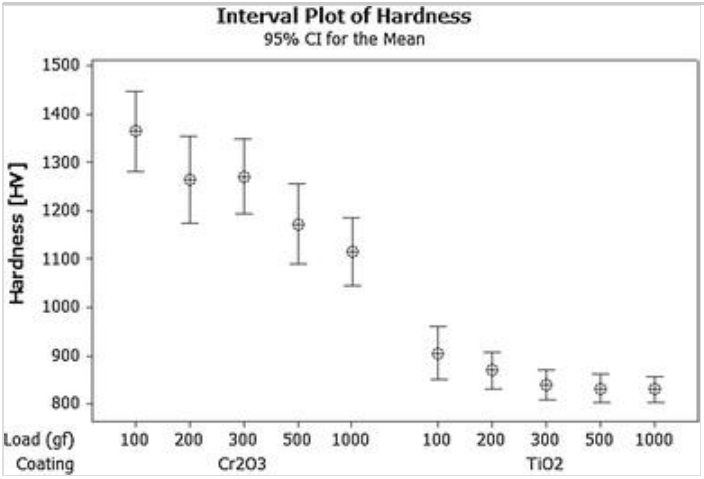

Both coatings were tested also at higher indentation loads. As Fig. 10 shows, while the indentation at 2 kg is still quite well defined in both coatings, when using a 30 kg load the Cr_2O_3 coating is severely damaged and the indentation cannot any more be measured (in fact, the behavior changes already between 3 and 5 kg). The TiO_2 coating shows mainly deformation accompanied by radial cracks. Naturally, the moderate thickness of the TiO_2-coating affects the shape of the indentation, but the ability of the ceramic coating to deform without large-scale brittle failure is nevertheless noteworthy.

Fig. 10

SEM images of Vickers indentations in the Cr_2O_3-coating with (a) HV_2 and (b) HV_{30}, and in the TiO_2-coating with (c) HV_2 and d) HV_{30}

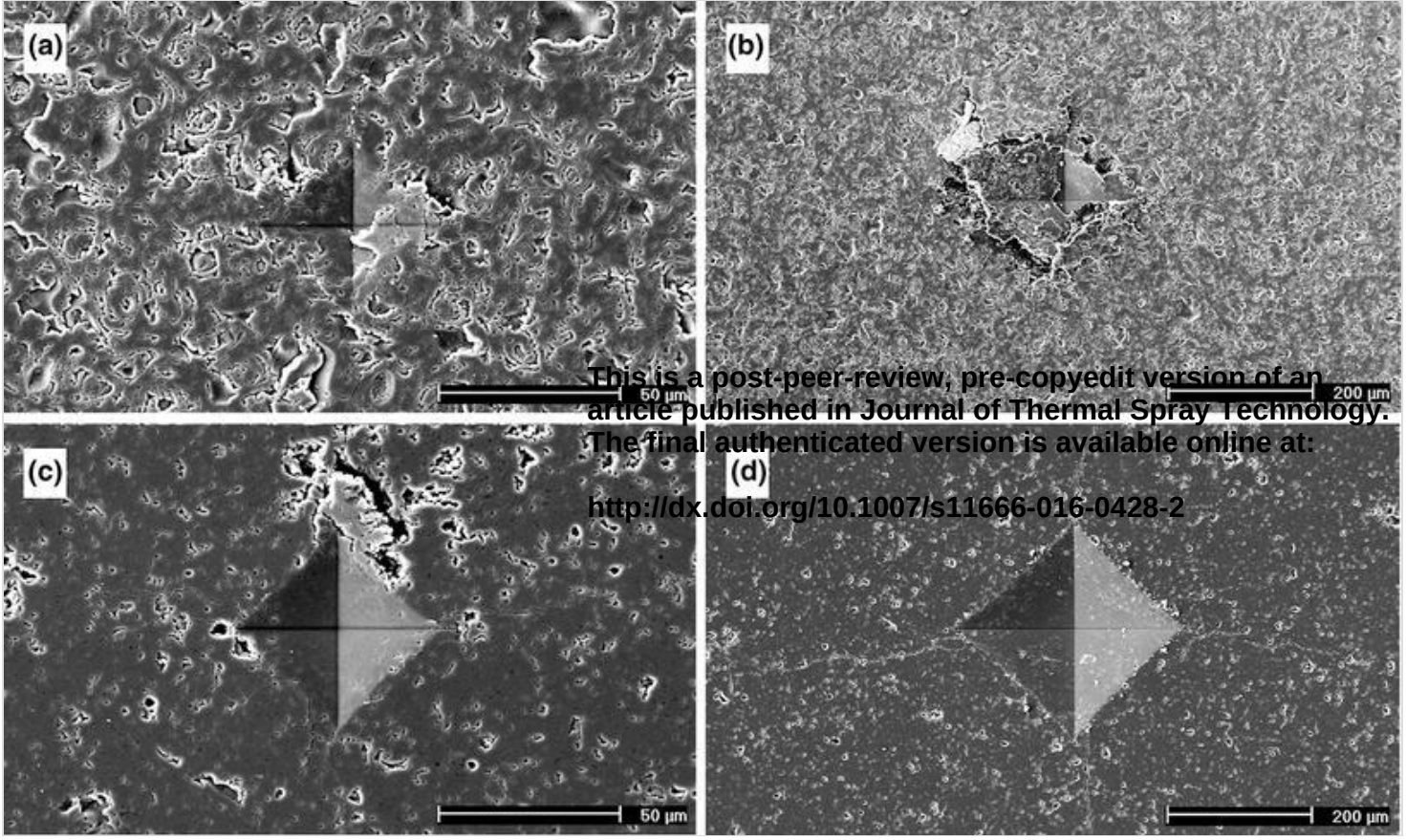

Similar behavior of the coatings under indentation with different loads further confirms that there indeed seems to be a threshold for a ceramic coating below which the hardness of the coating affects the impact energy absorbance more than the cohesion. Above this limit the structure of the coating seems to collapse, at least in the case of Cr_2O_3. However, further examinations are needed to more deeply understand this behavior. Some attempts have already been made for using the Weibull distribution in characterizing Vickers indentations with different loads on thermally sprayed ceramic coatings by Lima et al. (Ref 36), and a concept of brittleness as well as a threshold value for bulk ceramics have been suggested by Quinn et al. (Ref 37). Similar investigations would be beneficial for more materials and coatings manufactured with different coating methods. Both lower and higher impact energies should be used to verify that the threshold for the Cr_2O_3-coating indeed exists, as well as to possibly find such a threshold for TiO_2-coatings, too. A larger test matrix would also give more statistical significance to the findings.

Conclusions

Two plasma-sprayed ceramic coatings, Cr_2O_3 and TiO_2, were studied under high-velocity single impacts as well as with Vickers indentation experiments to characterize their deformation and failure mechanisms. The following observations and conclusions were made:

- The hardness of the coating seems to be able to deter the impacting projectile when the kinetic energy of the projectile is small, but with higher impact energies the cohesion of the coating becomes the determining factor.

- The Cr_2O_3-coating, with lower cohesion but higher hardness, is damaged less with small impact energies.

- The TiO_2-coating stayed largely intact with higher impact energies even with high degree of deformation of the substrate.

- The energy dissipation mechanism of thermally sprayed ceramic coatings in high-velocity impacts is mainly fracturing.

- The HVPI method proved a valuable experimental technique for the research of thermally sprayed ceramic coatings.

Acknowledgments

The work has been done within FIMECC Ltd and its HYBRIDS and PSA programmes. The authors gratefully acknowledge the financial support from Tekes (Finnish Funding Agency for Technology and Innovation) and the participating companies. The authors would like to thank Mr. Mikko Kylmälahti of Tampere University of Technology for spraying the coatings.

References

1. R.C. Tucker Jr., Introduction to Thermal Spray Technology, ASM. Handbook, C.M. Cotell, J.A. Sprague, F.A. Smidt Jr., Eds., *ASM Handbook, Volume 5A, Thermal Spray Technology*, R.C. Tucker Jr., Ed., ASM International, 2013, p 3-28.

2. P. Vuoristo, Thermal Spray Coating Processes, *Comprehensive Materials Processing*, S. Hashmi, G.F. Batalha, C.J. Van Tyne, B. Yilbas, Eds., Elsevier, 2014, p 229-276

3. H. Nakahira, Blast-furnace Tuyere Having Excellent Thermal Shock Resistance and High Durability, US3977660 A, 1976

4. G. Di Girolamo, E. Serra, Thermally Sprayed Nanostructured Coatings for Anti-wear and TBC Applications: State-of-the-art and Future Perspectives, *Anti-Abrasive Nanocoatings*, M. Aliofkhazraei, Ed., Woodhead Publishing Limited, 2015, p 513-541

5. L. Pawlowski, Applications of Coatings, *The Science and Engineering of Thermal Spray Coatings*, 2nd ed., John Wiley & Sons, 2008, p 543-596

6. E. Leivo, M. Vippola, P. Sorsa, P. Vuoristo, and T. Mäntylä, Wear and Corrosion Properties of Plasma Sprayed Al_2O_3 and Cr_2O_3 Coatings Sealed by Aluminum Phosphates, *J. Therm. Spray Technol.*, 1997, **2**(6), p 205-210

7. L.M. Berger, Titanium Oxide—New Opportunities for An Established Coating Material, *Thermal Spray 2004: Advances in Technology and Application, on CD-ROM, May 10-12, 2004 (Osaka, Japan)*, DVS-German Welding Society, 2004.

8. F. Toma, L. Berger, and C. Stahr, Microstructures and Functional Properties of Suspension-Sprayed Al_2O_3 and TiO_2 Coatings: An Overview, *J. Therm. Spray Technol.*, 2010, **1-2**(19), p 262-274

9. L.M. Berger, D.S. Saaro, D. Carl, C. Stahr, B.T. Fh-iws, and D. Sven, Development of Ceramic Coatings in the Cr_2O_3-TiO_2 System, *Therm. Spray Bull.*, 2009, **1**, p 64-77

10. A. Ibrahim, R.S. Lima, C.C. Berndt, and B.R. Marple, Fatigue and Mechanical Properties of Nanostructured and Conventional Titania (TiO_2) Thermal Spray Coatings, *Surf. Coat. Technol.*, 2007, **16-17**(201), p 7589-7596

11. M.W. Barsoum, *Fundamentals Of Ceramics*, 2nd ed., IOP Publishing, 2002, p 356-399

12. Y.X. Wang and S. Zhang, Toward Hard Yet Tough Ceramic Coatings, *Surf. Coat. Technol.*, 2014, **258**, p 1-16

13. P. Fauchais, G. Montavon, R.S. Lima, and B.R. Marple, Engineering a New Class of Thermal Spray Nano-Based Microstructures from Agglomerated Nanostructured Particles, Suspensions and Solutions: An Invited Review, *J. Phys. D Appl. Phys.*, 2011, **9**(44), p 1-53

14. L. Erickson, H. Hawthorne, and T. Troczynski, Correlations Between Microstructural Parameters, Micromechanical Properties and Wear Resistance of Plasma Sprayed Ceramic Coatings, *Wear*, 2001, **1-12**(250), p 569-575

15. R.S. Lima and B.R. Marple, From APS to HVOF Spraying of Conventional and Nanostructured Titania Feedstock Powders: A Study on the Enhancement of the Mechanical Properties, *Surf. Coat. Technol.*, 2006, **11**(200), p 3428-3437

16. J. Matejicek, S. Sampath, and J. Dubsky, X-ray Residual Stress Measurement in Metallic and Ceramic Plasma Sprayed Coatings, *J. Therm. Spray Technol.*, 1998, **4**(7), p 489-496

17. G. Bolelli, L. Lusvarghi, T. Varis, E. Turunen, M. Leoni, P. Scardi, C.L. Azanza-Ricardo, and M. Barletta, Residual Stresses in HVOF-Sprayed Ceramic Coatings, *Surf. Coat. Technol.*, 2008, **19**(202), p 4810-4819

18. A. Ang and C. Berndt, A Review of Testing Methods for Thermal Spray Coatings, *Int. Mater. Rev.*, 2014, **4**(59), p 179-223

19. J. Pina, A. Dias, and J.L. Lebrun, Study by X-ray Diffraction and Mechanical Analysis of the Residual Stress Generation During Thermal Spraying, *Mater. Sci. Eng., A*, 2003, **1-2**(347), p 21-31

20. I. Kleis, P. Kulu, Erosion Resistance of Powder Materials and Coatings, *Solid Particle Erosion: Occurrence, Prediction and Control*, Springer, 2008, p 129-168.

21. V. Matikainen, K. Niemi, H. Koivuluoto, and P. Vuoristo, Abrasion, Erosion and Cavitation Erosion Wear Properties of Thermally Sprayed Alumina Based Coatings, *Coatings*, 2014, **1**(4), p 18-36

22. R. Westergård, N. Axén, U. Wiklund, and S. Hogmark, An Evaluation of Plasma Sprayed Ceramic Coatings by Erosion, Abrasion and Bend Testing, *Wear*, 2000, **1-2**(246), p 12-19

23. L.C. Erickson, R. Westergård, U. Wiklund, N. Axén, H.M. Hawthorne, and S. Hogmark, Cohesion in Plasma-Sprayed Coatings—A Comparison Between Evaluation Methods, *Wear*, 1998, **1**(214), p 30-37

24. J. Takeuchi, H. Nakahira, J. Nagai, Physical Properties of Some Oxide Coatings by Low Pressure Plasma Spraying, *2nd Plasma Technik Symposium, Vol. 2*, S. Blum-Sandmeier, H. Eschnauer, P. Huber, A. Nicoll, Eds., June 5-7, 1991 (Lucerne, Switzerland), Plasma Technik AG, 1991

25. A.J. Sparks and I.M. Hutchings, Transitions in the Erosive Wear Behaviour of a Glass Ceramic, *Wear*, 1991, **1-2**(149), p 99-110

26. M. Lindroos, M. Apostol, V. Kuokkala, A. Laukkanen, K. Valtonen, K. Holmberg, and O. Oja, Experimental Study on the Behavior of Wear Resistant Steels Under High Velocity Single Particle Impacts, *Int. J. Impact Eng*, 2015, **78**, p 114-127

27. M. Lindroos, M. Apostol, V. Heino, K. Valtonen, A. Laukkanen, K. Holmberg, and V.-T. Kuokkala, The Deformation, Strain Hardening, and Wear Behavior of Chromium-Alloyed Hadfield Steel in Abrasive and Impact Conditions, *Tribol. Lett.*, 2015, **57**, p 1-11

28. E. Sarlin, M. Apostol, M. Lindroos, V.-T. Kuokkala, J. Vuorinen, T. Lepistö, and M. Vippola, Impact Properties of Novel Corrosion Resistant Hybrid Structures, *Compos. Struct.*, 2014, **108**, p 886-893

29. E. Sarlin, M. Lindroos, M. Apostol, V.T. Kuokkala, J. Vuorinen, T. Lepistö, and M. Vippola, The Effect of Test Parameters on the Impact Resistance of a Stainless Steel/Rubber/Composite Hybrid Structure, *Compos. Struct.*, 2014, **113**, p 469-475

30. R. Waudby, T. Varis, T. Suhonen, K. Holmberg, M. Apostol, M. Lindroos, V. Kuokkala, High Velocity Impact Testing of Thermal Spray Hard Carbide Coatings on Steel Substrates, *Proceedings of 5th World Tribology Congress WTC 2013*, September 8-13, 2013 (Torino, Italy), Politecnico di Torino, 2013

31. W. Molnar, S. Nugent, M. Lindroos, M. Apostol, and M. Varga, Ballistic and Numerical Simulation of Impacting Goods on Conveyor Belt Rubber, *Polym. Test.*, 2015, **42**, p 1-7

32. M. Apostol, V. Kuokkala, A. Laukkanen, K. Holmberg, R. Waudby, M. Lindroos, High Velocity Particle Impactor—Modeling and Experimental Verification of Impact Wear Tests, *Proceedings of 5th World Tribology Congress WTC 2013*, September 8-13, 2013 (Torino, Italy), Politecnico di Torino, 2013

33. S. Kuroda and T.W. Clyne, The Quenching Stress in Thermally Sprayed Coatings, *Thin Solid Films*, 1991, **1**(200), p 49-66

34. J. Leitner, K. Voleník, K. Neufuss, and B. Kolman, Vaporization of Components from Alloy Powder Particles in a Plasma Flow, *Czech J. Phys.*, 2006, **2**(56), p 1391-1400

35. C.B. Carter and M.G. Norton, *Fracturing: Brittleness, Ceramic Materials: Science and Engineering*, LLC, Springer Science + Business Media, 2007, p 325-339

36. R. Lima and B. Marple, High Weibull Modulus HVOF Titania Coatings, *J. Therm. Spray Technol.*, 2003, **2**(12), p 240-249

37. J.B. Quinn and G.D.G. Quinn, Indentation Brittleness of Ceramics: A Fresh Approach, *J. Mater. Sci.*, 1997, **16**(32), p 4331-4346